Correspondence to:
Y. C.-M. Liu,
liuyong@spaceweather.ac.cn

A multispacecraft study of a small flux rope entrained by rolling back magnetic field lines

Jia Huang[1,2], Yong C.-M. Liu[1], Jun Peng[1,2], Hui Li[1], Berndt Klecker[3], Charles J. Farrugia[4], Wenyuan Yu[4], Antoinette B. Galvin[4], Liang Zhao[5], and Jiansen He[6]

[1]State Key Laboratory of Space Weather, National Space Science Center, Chinese Academy of Sciences, Beijing, China, [2]College of Earth Sciences, University of Chinese Academy of Sciences, Beijing, China, [3]Max-Planck-Institut für extraterrestrische Physik, Garching, Germany, [4]Institute for the Study of Earth, Oceans and Space, University of New Hampshire, Durham, New Hampshire, USA, [5]Department of Climate and Space Sciences and Engineering, University of Michigan, Ann Arbor, Michigan, USA, [6]School of Earth and Space Sciences, Peking University, Beijing, China

Abstract We present a small flux rope (SFR) with smooth magnetic field rotations entrained by rolling back magnetic field lines around 1 AU. Such SFRs have only been seldom reported in the literature. This SFR was adjacent to a heliospheric plasma sheet (HPS), which is defined as a high plasma beta region in the vicinity of a heliospheric current sheet. Even though the SFR and HPS have different plasma beta, they possess similar plasma signatures (such as temperature, density, and bulk speed), density ratio of alpha particle-to-proton (N_α/N_p), and heavy ion ionization states, which imply that they may have a similar origin in the corona. The composition and the configuration of the rolling back magnetic field lines suggested that the SFR originated from the streamer belt through interchange reconnection. The origin processes of the SFR are presented here. Combining the observations of STEREO and ACE, the SFR was shown to have an axis tilted to the ecliptic plane and the radius may vary with different spatial positions. In this study, we suggest that interchange reconnection can play an important role for the origin of, at least, some SFRs and slow solar wind.

1. Introduction

Interplanetary magnetic flux ropes can be classified into two categories based on their spatial scales, the large-scale magnetic clouds (MCs, ~day) and the small-scale flux ropes (SFRs, ~hour) [*Cartwright and Moldwin*, 2008; *Tian et al.*, 2010]. The main criteria of SFRs [e.g., *Feng et al.*, 2015] include the following: the magnetic field configurations can be approximately described with constant force-free flux ropes, the durations are no more than 12 h, and their diameters are less than 0.2 AU. Generally, both SFRs and MCs [e.g., *Janvier et al.*, 2014a; *Feng et al.*, 2015] have similar bulk speed, proton density, and can be relatively well fitted with the Lundquist flux rope model [*Lundquist*, 1950]. Nevertheless, the SFRs differ from MCs not only in spatial and temporal scales but also in some other characteristics. The SFRs display a relatively higher proton temperature, lower magnetic field magnitude, and consequently larger plasma beta than that of MCs [*Janvier et al.*, 2014a]. *Yu et al.* [2014] further found that the proton temperature in small transients, an extended range of SFRs, is not significantly lower than the expected temperature, which is derived from the well-established correlation between the solar wind speed and temperature for normal solar wind expansion [*Richardson and Cane*, 1995, and references therein]. The large-scale MCs, which have been thoroughly studied, are associated with strong solar eruptions and drive major space weather events [e.g., *Lawrance et al.*, 2016; *Liu et al.*, 2016]. The origins of SFRs and their contributions to the slow solar wind have attracted much attention in recent years [*Moldwin et al.*, 2000; *Kilpua et al.*, 2009; *Rouillard et al.*, 2011; *Feng et al.*, 2015; *Yu et al.*, 2014, 2016].

The solar corona and interplanetary medium are believed to be the source regions for SFRs based on some statistical studies [e.g., *Mandrini et al.*, 2005; *Cartwright and Moldwin*, 2008; *Moore et al.*, 2010; *Janvier et al.*, 2014a, 2014b; *Feng et al.*, 2015; *Yu et al.*, 2016], but these studies generally provided indirect evidences. The SFRs are easily influenced by ambient solar wind because of their small sizes; therefore, it is important to remove the propagation effects to get direct proofs [*Janvier et al.*, 2014a; *Feng and Wang*, 2015]. *Mandrini et al.* [2005] first linked a sigmoid erupted from an X-ray point to a very small MC with a radius of 0.016 AU, i.e., SFR, based on multiinstrument and multiwavelength observations. *Rouillard et al.* [2009, 2011] confirmed the two source regions by tracing several SFRs back with remote sensing observations. Even though the imaging observations provide direct evidence, the accuracy of this method depends on

the Parker spiral propagation assumption and appropriate conditions (such as the SFRs should be entrained by corotating interaction regions), and the uncertainty of tracing the "very small flux ropes" (with an observed extent less than 0.05 AU) back to the Sun could be large [*Rouillard et al.*, 2010, 2011; *Janvier et al.*, 2014b]. In contrast, the heavy ion compositional measurements, such as the charge states and elemental abundance ratios, can link the in situ SFRs to their solar origins with high confidences [e.g., *von Steiger et al.*, 2000; *Zhao et al.*, 2009, 2014]. The heavy ion composition in the solar wind could provide information on the conditions at the origin and on the processes that act between there and the observing site [e.g., *Feldman et al.*, 1981; *von Steiger et al.*, 2000; *Zhao et al.*, 2009, 2014; *Song et al.*, 2016]. The charge states can be used as proxies for the coronal electron temperature (freezing-in temperature) because the ionization and recombination processes are frozen in below a certain height (1.5–3.5 solar radii) where the electron temperature is too low [*Hundhausen*, 1972; *Balogh et al.*, 2007]. The elemental abundance ratios associated with the first ionization potential (FIP) effect, which suggests the relative abundance ratio of low FIP elements (such as Fe) over high FIP elements (such as O), are enhanced in slow solar wind and MCs compared with fast solar wind [*Geiss*, 1982; *Fisk et al.*, 1999; *Wimmer-schweingruber and Hassler*, 2016]. In addition, the alpha particle-to-proton density ratio (N_α/N_p) is usually enhanced in MCs [*Lepri and Zurbuchen*, 2004; *Richardson and Cane*, 2004; *Feng and Wang*, 2015] but is depleted in the vicinity of the heliospheric current sheet (HCS), which is defined by the reversal of magnetic field polarity [e.g., *Gosling et al.*, 1981; *Crooker et al.*, 2004; *Li*, 2008; *Liu et al.*, 2014]. The depletions imply an origin from the closed field regions of the streamer belt [*Suess et al.*, 2009]. *Feng and Wang* [2015] have studied the compositional signatures of several SFRs and found some of them had enhanced N_α/N_p ($\geq$0.06), higher iron average charge states (Q<Fe> $\geq$ 12), and higher oxygen charge state ratio ($O^{7+}/O^{6+} \geq$ 1) than ambient solar wind, which are similar to those of MCs, implying that a number of SFRs have similar source regions as MCs. However, SFRs with different compositional signatures require further study.

The rolling back magnetic field lines, or "false polarity magnetic field lines" [e.g., *Kahler et al.*, 1996], are characterized by a separation between HCS and true sector boundary (TSB), which is defined by the inversion of the pitch angle distributions (PADs) of suprathermal electrons [e.g., *Foullon et al.*, 2009; *Liu et al.*, 2014]. Ideally, the HCS stays together with the TSB, but sometimes they are mismatched, implying most of the suprathermal electrons between them stream back to the Sun. Although some scientists explain the separation with magnetic islands [*Khabarova et al.*, 2015, 2016], it is generally accepted that the mismatch is caused by rolling back magnetic field lines [e.g., *Kahler et al.*, 1996; *Crooker et al.*, 2004; *Foullon et al.*, 2009]. Several studies also find that the rolling back magnetic field lines are closely related to interchange reconnection processes, which could occur at the streamer belt [*Wang et al.*, 2000; *Crooker et al.*, 2004], at pseudostreamers [*Owens et al.*, 2013], or between them [*Huang et al.*, 2016a, 2016b].

SFRs have been investigated during the last two decades. However, there are still many open questions. *Kilpua et al.* [2009] raised the question whether the SFRs that originate in the vicinity of the streamer belt could be released by reconnection at the streamer cusps and whether there exist SFRs related to false polarities which are expected in interchange reconnection debris. *Rouillard et al.* [2011] presented observations of such a case by tracing an erupting material continuously to 1 AU for the first time. However, this transient had no smooth magnetic field rotation, which they suggested to be associated with local kinks in the magnetic field lines. Nevertheless, the origin of such SFRs is still a puzzle.

In this work, we present a multispacecraft study of a SFR that is observed in the region where the magnetic field lines are rolling back. The compositional data are used to diagnose its origin, and the three-dimensional configuration of the SFR is also determined based on multispacecraft observations. We also develop a schematic model to explain its origin, and the implications to the origins of SFRs and slow solar wind are discussed.

In this paper, the data we used and multispacecraft observations of the case are presented in section 2. Discussion and conclusion are given in sections 3 and 4, respectively.

2. Data and Observations

In this study, STEREO and ACE data are used. The In-Situ Measurements of Particles and Coronal Mass Ejection Transients (IMPACT) suite [*Luhmann et al.*, 2008] and the Plasma and Suprathermal Ion Composition (PLASTIC) experiment [*Galvin et al.*, 2008] provide the in situ data from STEREO. The Magnetic Field Experiment (MAG)
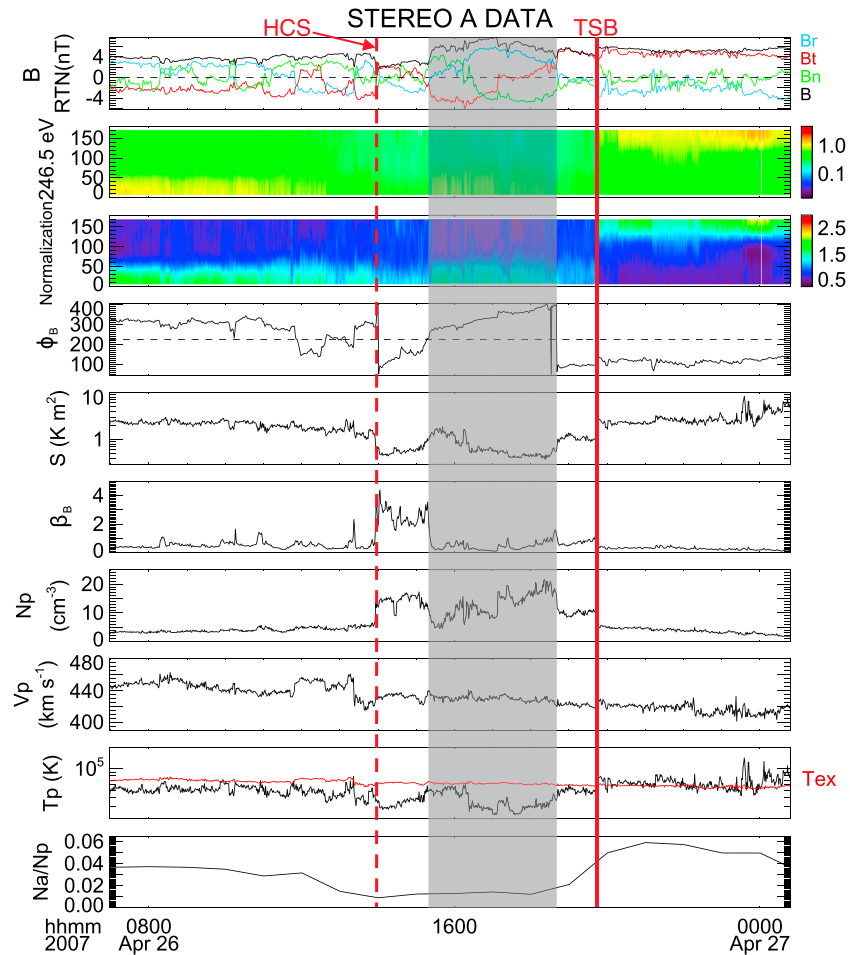
Figure 1. STEREO A (STA) observations on 26 April 2007. From top to bottom, the panels show the magnetic field components in RTN coordinates, the pitch angle distributions (PADs) of suprathermal electrons at an energy of 246.5 eV, the normalized PADs, the azimuthal angle of the magnetic field, the proton specific entropy, plasma beta, proton density, bulk speed, proton temperature, and alpha particles to proton density ratio (N_α/N_p). The red line in the ninth panel represents the expected temperature (for details see the text). The vertical dashed and solid lines denote the heliospheric current sheet (HCS) and the true sector boundary (TSB), respectively. The shaded region indicates the small flux rope (SFR).

[*Acuña et al.*, 2008] and the Solar Wind Electron Analyzer [*Sauvaud et al.*, 2008] of the IMPACT package measure the magnetic field and suprathermal electrons, respectively, and the PLASTIC experiment provides the plasma data. The STEREO data have a time resolution of 1 min. The ACE data are provided by three instruments. The Solar Wind Electron, Proton, and Alpha Monitor [*McComas et al.*, 1998] measures the in situ solar wind plasma and suprathermal electrons, the Magnetic Field Experiment (MAG) [*Smith et al.*, 1998] detects the magnetic field, and the Solar Wind Ion Composition Spectrometer [*Gloeckler et al.*, 1998] provides the solar wind composition measurements. The plasma data have a 64 s time resolution, the magnetic field data are obtained from 16 s data, and the compositional parameters are hourly averages.

2.1. STEREO A Observations

Figure 1 shows this special case observed by STEREO A (STA) on 26 April 2007. From top to bottom, the panels present the magnetic field components in RTN coordinates, the PADs of suprathermal electrons at an energy of 246.5 eV, the normalized PADs, the magnetic field azimuthal angle ϕ_B, the proton specific entropy $S = T_p/N_p^{2/3}$, plasma beta β_B, proton density, bulk speed, proton temperature, and N_α/N_p. The PAD is normalized in Figure 1 (second panel) by the mean value of all pitch angles at the same time. This method signifi-cantly improves the visualization of the PAD signatures without changing the data itself [*Huang et al.*, 2016a]. The vertical dashed line represents the HCS crossing at 13:58 UT, when ϕ_B flips from about 300° to
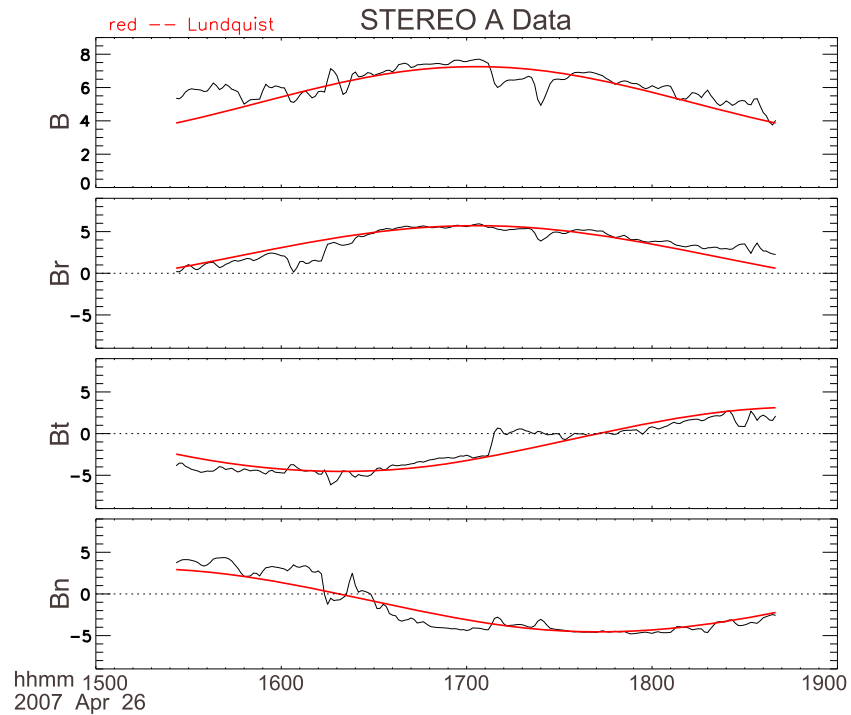
Figure 2. The Lundquist flux rope fitting results of the SFR observed by STA. The black lines represent the observed magnetic field components between 15:20 UT and 18:41 UT in RTN coordinates, and the red lines in each panel show the fitting results.

about 100°. A heliospheric plasma sheet (HPS), which is defined as a high β_B region [*Winterhalter et al.*, 1994], is also present following the HCS. The vertical solid line shows the TSB at 19:46 UT, when the PADs change from predominately 0° to 180°. The HCS is separated from the TSB by about 6 h, suggesting a group of rolling back magnetic field lines as introduced above.

The shaded region between 15:20 UT and 18:41 UT, characterized by a significant decrease of the entropy, marks the SFR lasting for less than 4 h. A smooth rotation of magnetic field components is evident in Figure 1 (first panel), and ϕ_B also evolves smoothly. Some studies found that some Alfvén wave trains might show observational magnetic field properties similar to SFRs [*Cartwright and Moldwin*, 2008; *Tian et al.*, 2010]. We exclude such a possibility for this SFR, using the method described by *Tian et al.* [2010], by correlating the RTN components of the Alfvén velocity fluctuations with the proton velocity perturbations. Because the correlation coefficients of their RTN components are only (0.004, −0.106, −0.369), they do not show the signature of Alfvénic fluctuations. Figure 2 presents the Lundquist flux rope fitting results for the magnetic field components during this time period. The black lines represent the observations of the magnetic field components, with total magnetic field strength and the three components in RTN coordinates shown from top to bottom plots, and the red lines denote the Lundquist fitting results. Obviously, the magnetic field components rotate smoothly and are fitted well by the modeled fields. The fit parameters give the SFR a radius (R_0) of 0.013 AU, and its axial direction is ($\phi = 319.2°$, $\theta = −35.3°$), where ϕ and θ are the longitude and latitude in the RTN coordinates. The fit suggests that STA crosses close to the axis of the SFR, with z_0/R_0 being 0.20, where z_0 is the distance of closest approach to the axis. In addition, the SFR is a right-handed flux rope and the estimated field strength at the axis is 7.46 nT.

Figure 1 shows several characteristics of this SFR: low β_B, slow speed of about 440 km s^{-1}, and enhanced density. Furthermore, the spatial extent of this SFR is about 0.035 AU as calculated with the observation time and solar wind speed, so it is indeed a very small flux rope [*Rouillard et al.*, 2011]. The red line in the temperature panel represents the expected temperature (T_{ex}) as calculated from the bulk speed with the formula, $T_{ex} = (0.027 \times V_p − 3.7)^2 \times 1000$, which is derived from the Wind data during 2007 to 2009 by *Yu et al.* [2014]. Inside the SFR, T_p/T_{ex} has a mean value of 0.58; i.e., T_p is smaller than T_{ex} but not as significantly
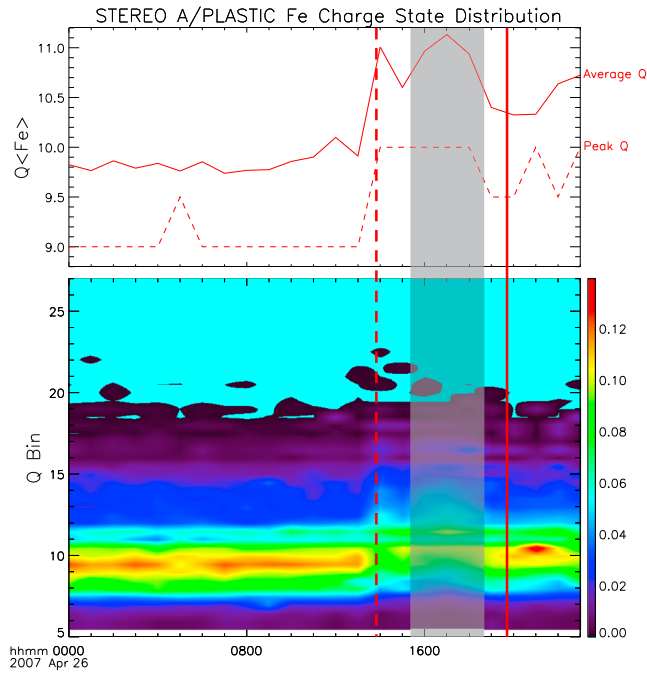
Figure 3. The iron charge states observed by STA/PLASTIC on 26 April 2007. The first panel shows the average (solid line) and peak (dashed line) charge states of iron. The second panel shows the fractional distribution of iron charge states. The vertical lines and shaded region have the same meanings as those in Figure 1.

smaller than in MCs ($T_p/T_{ex} \leq 0.5$) [*Richardson and Cane*, 1995], which is consistent with the characteristics of SFRs [*Yu et al.*, 2014]. In addition, N_α/N_p decreases to less than 0.02 within the SFR, suggesting that its source region should be the closed field region of the streamer belt [*Suess et al.*, 2009]. Moreover, between the HCS and the SFR there is a HPS. The similar characteristics of the SFR and HPS imply that they have similar origins. The time period between the end of the SFR and the TSB does not show a specific structure. The plasma parameters change from the signatures of the SFR to ambient slow solar wind values.

Besides N_α/N_p, the iron charge state distribution as shown in Figure 3 also reveals that the SFR and the HPS have a similar origin. The iron charge states are measured by PLASTIC onboard STA, and the time resolution is 1 h. Figure 3 (top) shows the average and peak charge states of iron,
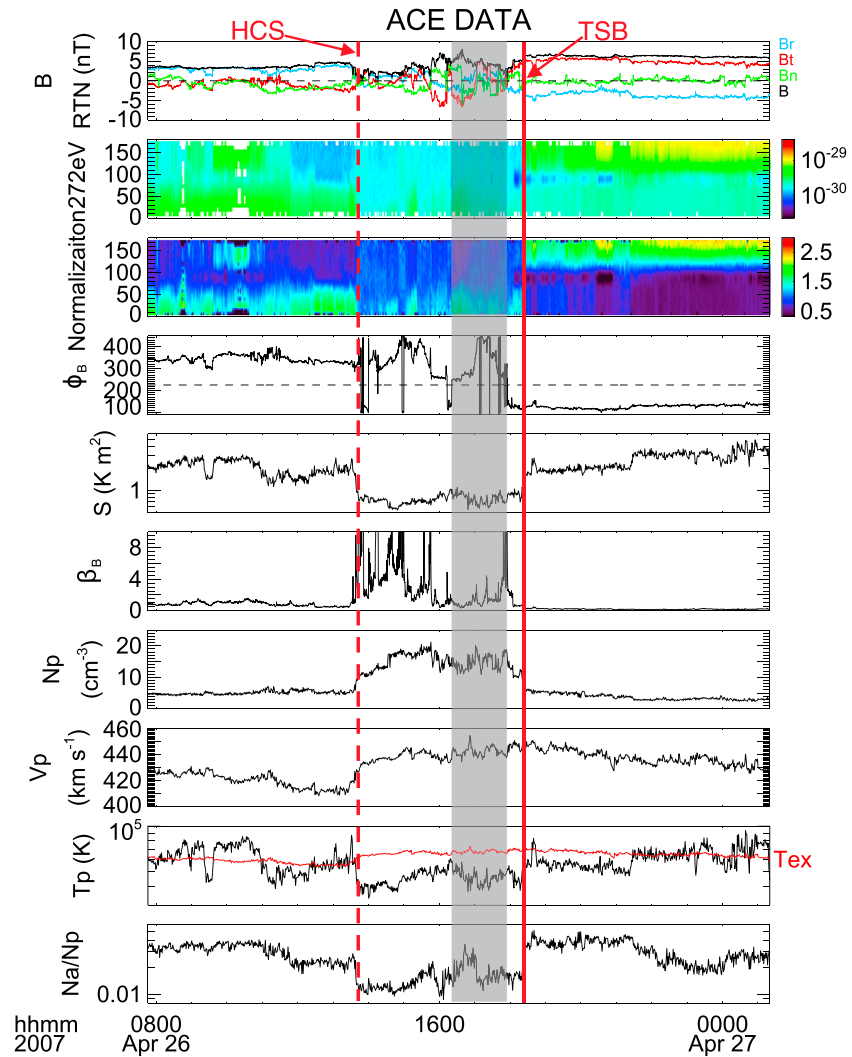
and the fractional distribution of iron charge states is presented in Figure 3 (bottom). The vertical lines and shaded region mark the same structures as in Figure 1. The iron charge distribution and Q<Fe> show that iron charge states are enhanced during the interval of rolling back magnetic field lines. The value of Q<Fe> increases to nearly the same level of about 11.0 in both HPS and SFR, in support of the identification of the two independent structures, and furthermore suggesting a similar source region of the HPS and SFR.

2.2. ACE Observations

Both ACE and Wind spacecraft in orbit around the L1 Lagrange point with heliocentric inertial (HCI) longitude and latitude separations from STA by only about (3.8°, 0.4°), and they observed similar structures. We present ACE observations because it provides also compositional data, although Wind has higher time resolution plasma data. Figure 4 shows the ACE observations on 26 April 2007, in the same format as Figure 1. Even though the magnetic field components and ϕ_B indicate much more complicated magnetic field variations, ACE observed a HPS with higher β_B and a SFR with lower β_B, similar to the observations of STA. These structures are consistent with two depletions as denoted by entropy, temperature, and even the higher time resolution data of N_α/N_p. The SFR was detected from 16:20 UT to 17:55 UT as marked by the shaded region. The boundaries of the SFR were principally selected based on both the plasma data and the sharp changes of ϕ_B. Note that we present values of ϕ_B less than 90° on top of Figure 4 (fourth panel). This shows that the azimuthal angle within the shaded region positively rotates continuously. In comparison, the SFR shows similar N_α/N_p and plasma characteristics as those observed by STA. But it has a much smaller spatial extent of only about 0.016 AU, implying that ACE might cross the SFR far from its axis and/or the SFR has a smaller radius at this position. Due to the short duration of the observations and the complicated magnetic field that could be caused by the interaction with ambient solar wind, this SFR is not suitable for the Lundquist fitting. Moreover, the TSB was evidently crossed at 18:21 UT as shown by the vertical solid line, but it is somewhat difficult to identify the HCS due to the confusing variations of ϕ_B. We prefer to locate the HCS at 13:45 UT as shown by the vertical dashed line for several reasons. On one hand, ϕ_B flips from about 320° to 140°,

Figure 4. ACE observations on 26 April 2007, in the same format as Figure 1. The values of ϕ_B with less than 90° are shown on the top of the fourth panel.

which is sharper than other flips. On the other hand, the HCS generally lies at the edges of the N_α/N_p depletion zone [*Suess et al.*, 2009]. Furthermore, the HCS leads the HPS here, which is similar to STA observations, and it is also consistent with former studies that HPSs tend to retain their relative positions with respect to HCSs at around 1 AU [*Liu et al.*, 2014].

Figure 5 shows the compositional data of ACE between 08:00 UT and 22:00 UT on 26 April 2007. From top to bottom, the panels show O^{7+}/O^{6+} ratio, carbon charge state ratio (C^{6+}/C^{5+}), average oxygen charge states ($Q\langle O\rangle$), average carbon charge states ($Q\langle C\rangle$), $Q\langle Fe\rangle$, and iron abundance ratios (Fe/O). Figure 5 (sixth panel) is related to the FIP effect, and the other panels are related to the freezing-in temperature. The vertical lines and shaded region mark the same structures as in Figure 4. In the top five panels, the ionization states within both the SFR and HPS increase to a similar higher level than in the ambient solar wind, which is similar to the $Q\langle Fe\rangle$ values observed by STA. Therefore, the compositional data of ACE also support the identification of the structures and, again, suggest a similar origin of the HPS and SFR. Furthermore, the Fe/O ratio is higher in the HPS than that in SFR, which implies that the SFR may emerge on a smaller loop at the origin [*von Steiger et al.*, 2000]. We note that the variation of $Q\langle Fe\rangle$ observed by ACE was somewhat different from the variation of other ionization states observed by both ACE and STA. The variations of ionization states of heavy ions are expected to be consistent to a certain extent. However, iron charge states may vary rapidly at
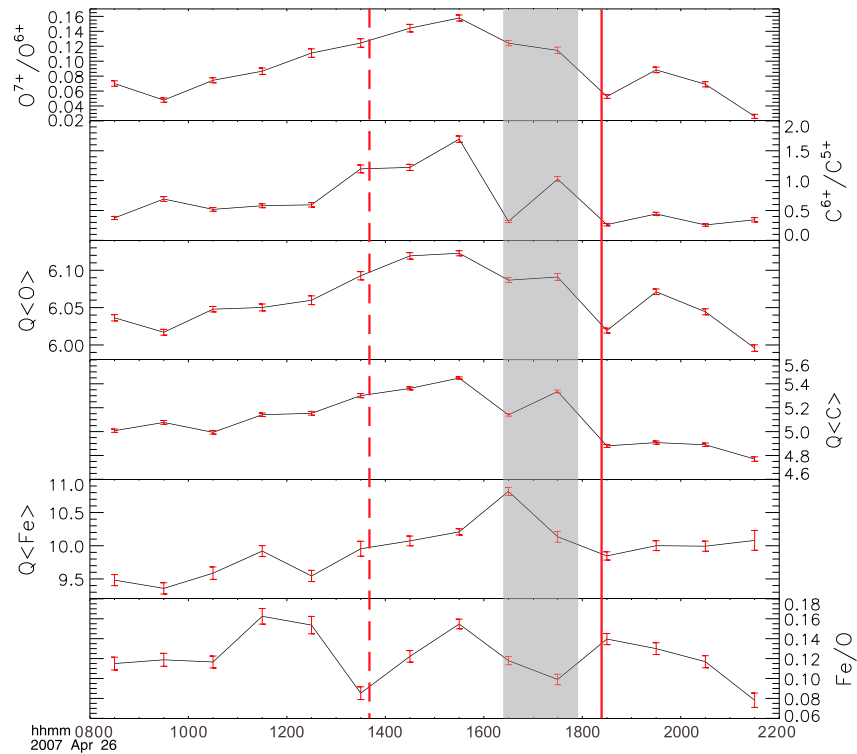
Figure 5. The compositional measurements observed by ACE during 08:00 UT to 21:00 UT on 26 April 2007. From top to bottom, the panels present O^{7+}/O^{6+}, C^{6+}/C^{5+}, Q<O>, Q<C>, Q<Fe>, and Fe/O, which are described in the text. One sigma error bars are added for each data point with red color. The vertical lines and shaded region have the same meanings as those in Figure 4.

the source regions on different spatial scales [*von Steiger et al.*, 2000]. Thus, the mismatch may be caused by the nonuniform distributions of Q<Fe> within SFR. Nevertheless, the ionization states are similar in both HPS and SFR, supporting our conclusion that they have similar origins.
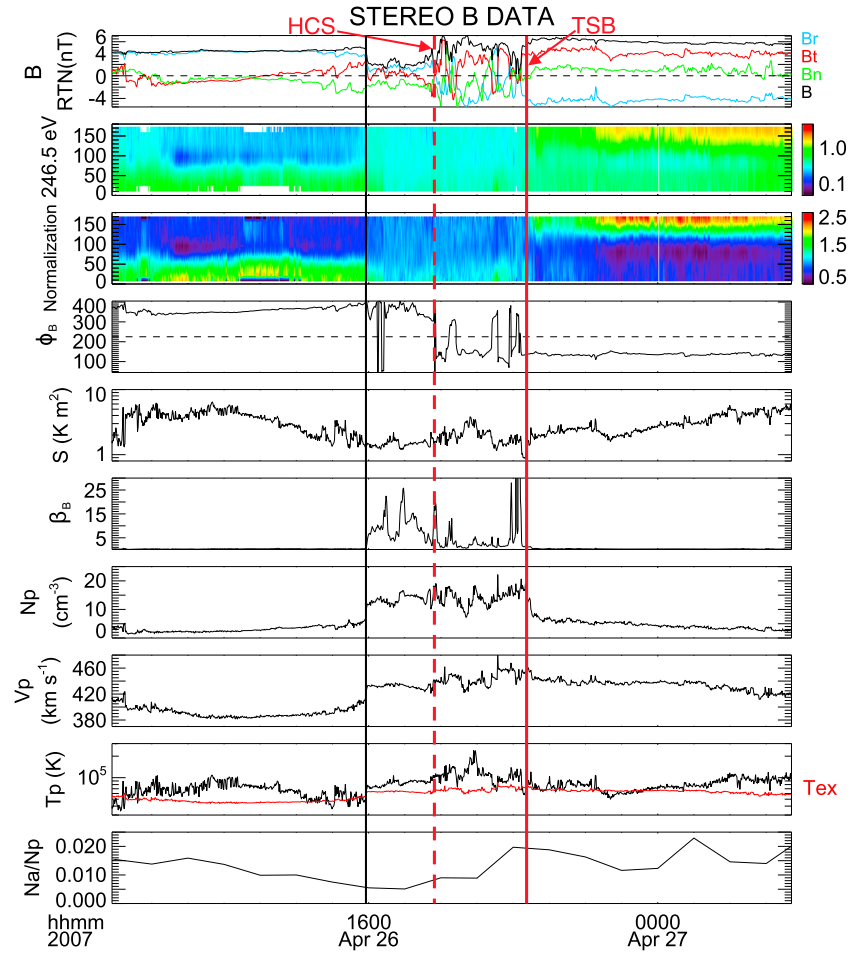
2.3. STEREO B Observations

We also studied observations of STEREO B (STB), which is separated from ACE in HCI longitude and latitude by about 1.7° and 0.4°, respectively. Figure 6 shows the STB observations on 26 April 2007, in the same format as Figure 1. Apparently, STB observed structures different from STA and ACE. The vertical dashed line marks the HCS at 17:50 UT, when ϕ_B flips from about 300° to 120°. The TSB was observed at 20:30 UT, as indicated by the red vertical solid line. Between the black vertical line and the HCS is a HPS, characterized by a high β_B region, which started at 15:55 UT. Compared with observations by STA and ACE, STB observed quite different values of entropy, temperature, and N_α/N_p. Neither the entropy nor the N_α/N_p values show a decrease during this time, and T_p is even larger than T_{ex} as shown in the ninth panel. Besides, there is no magnetic field configurations that show similar rotations as those defining the SFR observed by STA and ACE during this time. In addition, a radial magnetic field structure, which is defined by the radial component having more than 90% of the total strength [e.g., *Gosling and Skoug*, 2002; *Wang et al.*, 2003], was observed from 08:50 UT to 15:05 UT. However, STA and ACE did not observe such a structure.

3. Discussion

3.1. Spatial Morphology of the SFR

The observations suggest both STA and ACE have encountered the SFR, but STB did not. The fitting results and observation timing of the SFR indicate that STA may cross closer to the axis, while ACE probably crosses near the boundary of the SFR. In the following we will discuss the spatial morphology of this SFR in more detail.

Figure 6. STEREO B observations on 26 April 2007, in the same format as Figure 1. The red vertical dashed and solid line represent the HCS and TSB, respectively. Between the black vertical line and the HCS is a heliospheric plasma sheet (HPS).
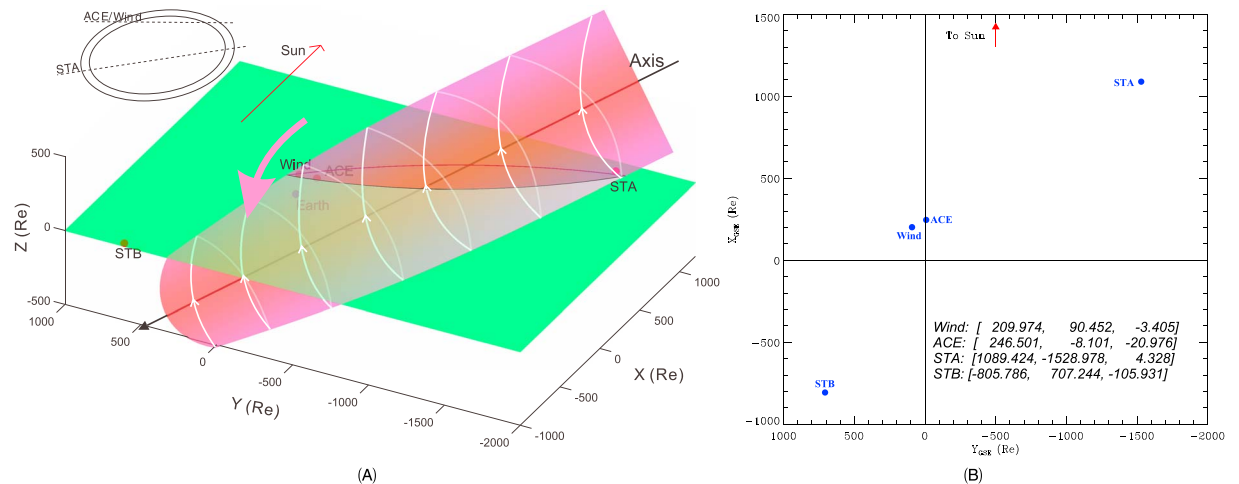
Figure 7. (a) The spatial morphology of the SFR. The details are presented in the text. (b) The spacecraft positions in the ecliptic plane (GSE coordinates in Earth radii (R_E)). The blue dots indicate the spacecraft positions with their names following, and the right bottom presents their detailed positions in units of R_E.

Figure 7a shows a simplified morphology of this SFR based on the observations and Lundquist fitting results. Figure 7b denotes the spacecraft positions in the ecliptic plane, with the data obtained from SSCWeb (http://sscweb.gsfc.nasa.gov) at 12:00 UT on 26 April 2007. The green plane represents the ecliptic plane, and the magenta cylinder shows the SFR, with the black arrow and the helical lines with white arrow indicating the orientation of the magnetic field. The propagation direction of the SFR is suggested by the magenta arrow, which mainly points $-x$ direction (GSE coordinate) and also $-y$ direction as the solar wind affects. The intersection of the helical magnetic field with the ecliptic plane is marked by a black ellipse. The axis of the SFR is tilted by about $-35°$ as the fitting results of STA show, and the radius varies with spatial positions. The top left insert shows the projected intersection of the SFR where the spacecraft pass through, with STA being close to the axis but ACE/Wind being far from the axis. The crossing site of SFR may make the trajectory (dashed line) of ACE/Wind not parallel to that of STA. The different sizes of the projected sections correspond to the possibly different radii of the SFR at different positions. This figure shows that the separation between ACE and STA is mainly in the GSE x direction and y direction. The separation in the x direction together with the near-simultaneous entry into the SFR of both spacecraft is explained by the fitted longitude of the SFR axis. The fact that ACE crosses far away from axis and STA near axis is consistent with the latitude of the SFR axis inferred from the fitting. Based on the positions of the spacecraft as shown in Figure 7b and the solar wind speed [*Opitz et al.*, 2009; *Simunac et al.*, 2009], and assuming a quasi-stationary structure, we can estimate that STA should lag ACE and STB by about 2.3 h and 1.9 h, respectively, if we take the TSB as reference. However, the observations of the TSB show that STA lags ACE by about 1.5 h but leads STB by about 0.7 h. This result further supports that STB observes other structures than STA and ACE.

3.2. Origins of the SFR

The origin of very small flux ropes are rarely identified with direct evidence due to their faint appearances in the imaging observations, and they are also easily influenced by ambient solar wind [*Rouillard et al.*, 2011; *Janvier et al.*, 2014a]. Furthermore, there are still disputes on the release mechanism for the SFRs that originate from the streamer belt. Some studies suggest that these SFRs, or the so-called "plasma blobs" [e.g., *Sheeley et al.*, 1997; *Song et al.*, 2009], are released from the cusp of streamers by interchange reconnection [*Wang et al.*, 2000]. However, some simulation results suggest that they are pinched off by the intrinsic instability driven magnetic reconnection processes [*Chen et al.*, 2009]. The study of this special case may provide some clues to these open questions.

The peculiar magnetic field configurations and compositional signatures provide some insight into the origin of this SFR. First, STA observations indicate that the SFR is entrained by the rolling back magnetic field lines. In general, the rolling back magnetic field lines are caused by interchange reconnection processes between closed and open magnetic field lines [*Crooker et al.*, 2004; *Foullon et al.*, 2009; *Owens et al.*, 2013]. Second, the similar level of ionization states and N_α/N_p of the SFR and HPS suggest a similar origin, i.e., the closed field region of the streamer belt. Third, the unidirectional suprathermal electrons infer that this SFR is still rooted with one foot at the Sun [e.g., *Feng et al.*, 2015], which also implies that this SFR cannot be a detached plasmoid [*Foullon et al.*, 2011] that pinched off as described by *Chen et al.* [2009]. Furthermore, the suprathermal electrons still flow antisunward, which is different from those in the rolling back magnetic field lines, implying that this SFR may not have formed at the same time as the rolling back magnetic field lines.

Figure 8 is presented to illustrate a possible origin of this SFR, based on the above analysis and STA observations. In this figure, the yellow circles represent the Sun and the black arrows show the polarity of the magnetic field lines. Figure 8a shows the streamer belt. Figures 8b and 8c indicate the interchange reconnection process, taking place between the closed loop and an adjacent, noncoplanar open magnetic field line [e.g., *Wang et al.*, 2000; *Crooker et al.*, 2004]. Then, the rolling back magnetic field lines form as shown by the red arrows in Figure 8d, evidenced by the sunward streaming suprathermal electrons. The dashed lines indicate that these magnetic field lines may not lie in the same plane. Figure 8e shows the SFR, which is illustrated by the orange helical lines, released immediately after the formation of the rolling back magnetic field lines. This can be inferred from the Fe/O observations, which imply that the SFR should be formed on a relatively smaller loop than HPS. We propose that this SFR is also released through interchange reconnection with the same processes as shown in Figures 8b and 8c. The difference is that these magnetic field lines are twisted, which could be formed prior to or during its releasing process [e.g., *Song et al.*, 2016, and references therein]. The dash-dotted line indicates that the SFR is still magnetically connected to the Sun, but whether the leg is
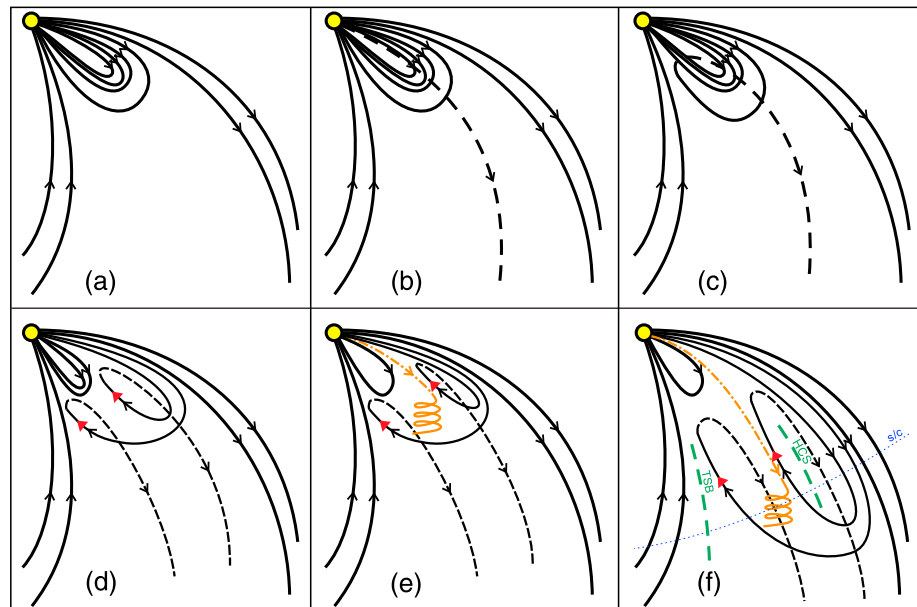
Figure 8. A schematic illustrating the origin of the SFR based on the STA observations. The details are presented in the text.

also twisted is still not known, even for large-scale MCs [e.g., *Owens*, 2016; *Wang et al.*, 2016]. Figure 8f indicates the topology at 1 AU: this SFR is entrained by the rolling back magnetic field lines and passes over STA. The green lines represent the HCS and TSB observed by STA, and the dotted line represents the trajectory of the spacecraft. This configuration fits well with the STA observations. Furthermore, it also suggests that this SFR may not be formed within the HCS in the interplanetary medium. If it had been formed through magnetic reconnection within the HCS, then the rolling back magnetic field lines in the leading side that contain the HCS would disappear after the reconnection process or at least would not show up in the leading side of the SFR. This also suggests that, at least, some SFRs in the vicinity of HCSs may not be formed at the HCSs in the interplanetary space, which is different from the conclusion suggested by *Feng et al.* [2015].

3.3. Implications and Other Concerns

The SFR entrained by rolling back magnetic field lines has important implications. In this special case, the SFR and an adjacent HPS present similar N_α/N_p and compositional signatures, implying that this SFR originates from the streamer belt, which is consistent with previous conclusion that mainly inferred from the peculiar configurations of the rolling back magnetic field lines. Our results show that heavy ion composition can be used as an effective tool to diagnose the source regions of very small flux ropes. This special case in our study further indicates that the interchange reconnection may also be responsible for some SFR formation process. However, there is no clear signal of magnetic reconnection processes in the Nançay Radioheliograph observations [*Kerdraon and Delouis*, 1997], which allow imaging of weak energy release at coronal heights [*Mandrini et al.*, 2014]. This could be caused by the weak eruption signatures of this SFR due to its very small size. Therefore, more case studies in the future are necessary to link this kind of SFRs to interchange reconnection processes and find out whether some SFRs could be formed in the heliosphere medium. Furthermore, STA observations suggest that the very small flux ropes could sustain their smooth magnetic field rotations during the propagation to 1 AU, even if the rotations may be disturbed by local kinks in the magnetic field lines [*Rouillard et al.*, 2011] or by the interaction with ambient solar wind as ACE observations show. Considering that this kind of SFRs or plasma blobs contribute significantly to the slow solar wind, we suggest that at least some slow solar wind could have a similar origin mechanism.

The kind of SFRs as studied in this paper seems to have a low occurrence rate. We have searched for them during 2007 to 2010 with STEREO data, but only this case shows good characteristics. There could be several reasons for this. First, the rolling back magnetic field lines also have a low occurrence rate

[*Crooker et al.*, 2004]. Second, the plasma blobs, which are important sources of this kind SFRs, are released with a rate of 3–5 per day in the solar minimum [*Wang et al.*, 1998; *Song et al.*, 2009]. Third, both the rolling back magnetic field lines and the SFRs are sensitive to the interactions with ambient solar wind. It is difficult to identify them with changing magnetic field configurations. Besides, the small extents and spatial morphologies of the SFRs make them hard to be captured by spacecraft, as suggested by STB observations in this case. Therefore, the low occurrence rate of the entrainment is reasonable.

4. Conclusion

In this study, we present a SFR, which has smooth magnetic field rotations, entrained by rolling back magnetic field lines around 1 AU. This SFR shows similar plasma signatures, N_α/N_p depletions, and ionization states as the HPS, implying that they may have a similar origin. Combining the compositional signatures and the peculiar magnetic field configurations, we suggest that this SFR should be released from the streamer belt through interchange reconnection. Based on the multiple spacecraft observations, we found that this type of SFR may be easily missed, due to its small size and spatial morphology. This SFR is classified as a very small flux rope, which can be hardly traced back to their origins where the remote sensing observations are available to compare. However, we suppose that the compositional signature is an effective diagnostic to study the origins of such SFRs as well as the ones that could be traced back. Besides, although this is a study of a special case, it may still help us modify some former views: interchange reconnection may be responsible for the origin of some SFRs, and at least some SFRs in the vicinity of HCSs should not be formed in the interplanetary medium. There are still open questions which need to be addressed, such as the relationship between the SFR and the radial magnetic field structure, and the evolution of the SFR axis during its propagation.

References

Acuña, M. H., D. Curtis, J. L. Scheifele, C. T. Russell, P. Schroeder, A. Szabo, and J. G. Luhmann (2008), The STEREO/IMPACT magnetic field experiment, in *The STEREO Mission*, edited by C. T. Russell, pp. 203–226, Springer, New York, doi:10.1007/978-0-387-09649-0_8.

Balogh, A., L. J. Lanzerotti, and S. T. Suess (2007), *The Heliosphere Through the Solar Activity Cycle*, pp. 53–62, Springer, Chichester, U. K.

Cartwright, M. L., and M. B. Moldwin (2008), Comparison of small-scale flux rope magnetic properties to large-scale magnetic clouds: Evidence for reconnection across the HCS?, *J. Geophys. Res.*, 113, A09105, doi:10.1029/2008JA013389.

Chen, Y., X. Li, H. Q. Song, Q. Q. Shi, S. W. Feng, and L. D. Xia (2009), Intrinsic instability of coronal streamers, *Astrophys. J.*, 691(2), 1936, doi:10.1088/0004-637X/691/2/1936.

Crooker, N. U., S. W. Kahler, D. E. Larson, and R. P. Lin (2004), Large-scale magnetic field inversions at sector boundaries, *J. Geophys. Res.*, 109, A03108, doi:10.1029/2003JA010278.

Feldman, W. C., J. R. Asbridge, S. J. Bame, E. E. Fenimore, and J. T. Gosling (1981), The solar origin of solar interstream flows: Near equatorial coronal streamers, *J. Geophys. Res.*, 86, 5408–5416, doi:10.1029/JA086iA07p05408.

Feng, H. Q., and J. M. Wang (2015), Observations of several unusual plasma compositional signatures within small interplanetary magnetic flux ropes, *Astrophys. J.*, 809, 112.

Feng, H. Q., G. Q. Zhao, and J. M. Wang (2015), Counterstreaming electrons in small interplanetary magnetic flux ropes, *J. Geophys. Res. Space Physics*, 120, 10,175–10,184, doi:10.1002/2015JA021643.

Fisk, L. A., T. H. Zurbuchen, and N. A. Schwadron (1999), On the coronal magnetic field: Consequences of large-scale motions, *Astrophys. J.*, 521, 868–877.

Foullon, C., et al. (2009), The apparent layered structure of the heliospheric current sheet: Multi-spacecraft observations, *Sol. Phys.*, 259(1–2), 389–416, doi:10.1007/s11207-009-9452-4.

Foullon, C., et al. (2011), Plasmoid releases in the heliospheric current sheet and associated coronal hole boundary layer evolution, *Astrophys. J.*, 737, 16, doi:10.1088/0004-637X/737/1/16.

Galvin, A. B., et al. (2008), The plasma and suprathermal ion composition (PLASTIC) investigation on the STEREO observatories, *Space Sci. Rev.*, 136(1–4), 437–486, doi:10.1007/s11214-007-9296-x.

Geiss, J. (1982), Processes affecting abundances in the solar wind, *Space Sci. Rev.*, 33, 201–217.

Gloeckler, G., et al. (1998), Investigation of the composition of solar and interstellar matter using solar wind and pickup ion measurements with SWICS and SWIMS on the ACE spacecraft, *Space Sci. Rev.*, 86, 497–539, doi:10.1023/A:1005036131689.

Gosling, J. T., G. Borrini, J. R. Asbridge, S. J. Bame, W. C. Feldman, and R. T. Hansen (1981), Coronal streamers in the solar wind at 1 AU, *J. Geophys. Res.*, 86(A7), 5438–5448, doi:10.1029/JA086iA07p05438.

Gosling, J. T., and R. M. Skoug (2002), On the origin of radial magnetic fields in the heliosphere, *J. Geophys. Res.*, 107(A10), 1327, doi:10.1029/2002JA009434.

Huang, J., Y. C.-M. Liu, B. Klecker, and Y. Chen (2016a), Coincidence of heliospheric current sheet and stream interface: Implications for the origin and evolution of the solar wind, *J. Geophys. Res. Space Physics*, 121, 19–29, doi:10.1002/2015JA021729.

Huang, J., Y. C.-M. Liu, Z. Qi, B. Klecker, O. Marghitu, A. B. Galvin, C. J. Farrugia, and X. Li (2016b), A multievent study of the coincidence of heliospheric current sheet and stream interface, *J. Geophys. Res. Space Physics*, 121, 10,768–10,782, doi:10.1002/2016JA022842.

Hundhausen, A. J. (1972), *Coronal Expansion and Solar Wind*, Phys. Chem. Space, vol. 5, pp. 94–121, Springer, New York.

Janvier, M., P. Démoulin, and S. Dasso (2014a), In situ properties of small and large flux ropes in the solar wind, *J. Geophys. Res. Space Physics*, 119, 7088–7107, doi:10.1002/2014JA020218.

Janvier, M., P. Démoulin, and S. Dasso (2014b), Are there different populations of flux ropes in the solar wind?, *Sol. Phys.*, 289, 2633–2652, doi:10.1007/s11207-014-0486-x.

Kerdraon, A., and J.-M. Delouis (1997), The Nançay Radioheliograph, in *Coronal Physics From Radio and Space Observations, Lecture Notes in Physics*, vol. 483, edited by G. Trottet, pp. 192–201, Springer, Berlin.

Khabarova, O., G. P. Zank, G. Li, J. A. le Roux, G. M. Webb, A. Dosch, and O. E.. Malandraki (2015), Small-scale magnetic islands in the solar wind and their role in particle acceleration. I. Dynamics of magnetic islands near the heliospheric current sheet, *Astrophys. J.*, *808*, 181, doi:10.1088/0004-637X/808/2/181.

Khabarova, O., G. P. Zank, G. Li, O. E. Malandraki, J. A. le Roux, and G. M. Webb (2016), Small-scale magnetic islands in the solar wind and their role in particle acceleration. II. Particle energization inside magnetically confined cavities, *Astrophys. J.*, *827*, 122, doi:10.3847/0004-637X/827/2/122.

Kahler, S. W., N. U. Crocker, and J. T. Gosling (1996), The topology of intrasector reversals of the interplanetary magnetic field, *J. Geophys. Res.*, *101*(A11), 24,373–24,382, doi:10.1029/96JA02232.

Kilpua, E. K. J., et al. (2009), Small solar wind transients and their connection to the large-scale coronal structure, *Sol. Phys.*, *256*, 327–344.

Lawrance, M. B., A. Shanmugaraju, Y. J. Moon, M. S. Ibrahim, and S. Umapathy (2016), Relationships between interplanetary coronal mass ejection characteristics and geoeffectiveness in the rising phase of solar cycles 23 and 24, *Sol. Phys.*, *291*(5), 1547–1560.

Lepri, S. T., and T. H. Zurbuchen (2004), Iron charge state distributions as an indicator of hot ICMEs: Possible sources and temporal and spatial variations during solar maximum, *J. Geophys. Res.*, *109*, A01112, doi:10.1029/2003JA009954.

Li, G. (2008), Identifying current-sheet–like structures in the solar wind, *Astrophys. J.*, *672*, L65–L68.

Liu, Y. C.-M., et al. (2014), A statistical analysis of heliospheric plasma sheets, heliospheric current sheets, and sector boundaries observed in situ by STEREO, *J. Geophys. Res. Space Physics*, *119*, 8721–8732, doi:10.1002/2014JA019956.

Liu, Y. D., H. Hu, C. Wang, J. G. Luhmann, J. D. Richardson, Z. Yang, and R. Wang (2016), On Sun-to-Earth propagation of coronal mass ejections: II. Slow events and comparison with others, *Astrophys. J. Suppl. Ser.*, *222*(2), 23.

Luhmann, J. G., et al. (2008), STEREO IMPACT investigation goals, measurements, and data products overview, *Space Sci. Rev.*, *136*(1–4), 117–184, doi:10.1007/s11214-007-9170-x.

Lundquist, S. (1950), Magnetohydrostatic fields, *Ark. Fys.*, *2*, 361–365.

Mandrini, C. H., et al. (2005), Interplanetary flux rope ejected from an X-ray bright point. The smallest magnetic cloud source-region ever observed, *Astron. Astrophys.*, *434*, 725–740, doi:10.1051/0004-6361:20041079.

Mandrini, C. H., et al. (2014), How can active region plasma escape into the solar wind from below a closed helmet streamer?, *Sol. Phys.*, *289*, 4151, doi:10.1007/s11207-014-0582-y.

McComas, D. J., S. J. Bame, P. Barker, W. C. Feldman, J. L. Phillips, P. Riley, and J. W. Griffee (1998), Solar wind electron proton alpha monitor (SWEPAM) for the Advanced Composition Explorer, *Space Sci. Rev.*, *86*, 563–612, doi:10.1023/A:1005040232597.

Moldwin, M. B., S. Ford, R. Lepping, J. Slavin, and A. Szabo (2000), Small-scale magnetic flux ropes in the solar wind, *Geophys. Res. Lett.*, *27*(1), 57–60, doi:10.1029/1999GL010724.

Moore, R. L., J. W. Cirtain, A. C. Sterling, and D. A. Falconer (2010), Dichotomy of solar coronal jets: Standard jets and blowout jets, *Astrophys. J.*, *720*, 757–770, doi:10.1088/0004-637X/720/1/757.

Opitz, A., et al. (2009), Temporal evolution of the solar wind bulk velocity at solar minimum by correlating the STEREO A and B PLASTIC measurements, *Sol. Phys.*, *256*, 365–377, doi:10.1007/s11207-008-9304-7.

Owens, M. J. (2016), Do the legs of magnetic clouds contain twisted flux-rope magnetic fields?, *Astrophys. J.*, *818*(2), 197.

Owens, M. J., N. U. Crocker, and M. Lockwood (2013), Solar origin of heliospheric magnetic field inversions: Evidence for coronal loop opening within pseudostreamers, *J. Geophys. Res. Space Physics*, *118*, 1868–1879, doi:10.1002/jgra.50259.

Richardson, I. G., and H. V. Cane (1995), Regions of abnormally low proton temperature in the solar wind (1965–1991) and their association with ejecta, *J. Geophys. Res.*, *100*(A12), 23,397–23,412, doi:10.1029/95JA02684.

Richardson, I. G., and H. V. Cane (2004), Identification of interplanetary coronal mass ejections at 1 AU using multiple solar wind plasma composition anomalies, *J. Geophys. Res.*, *109*, A09104, doi:10.1029/2004JA010598.

Rouillard, A. P., et al. (2009), A multispacecraft analysis of a small-scale transient entrained by solar wind streams, *Sol. Phys.*, *256*(1–2), 307.

Rouillard, A. P., et al. (2010), Intermittent release of transients in the slow solar wind: 1. Remote sensing observations, *J. Geophys. Res.*, *115*, A04103, doi:10.1029/2009JA014471.

Rouillard, A. P., et al. (2011), The solar origin of small interplanetary transients, *Astrophys. J.*, *734*, doi:10.1088/0004-637X/734/1/7.

Sauvaud, J. A., et al. (2008), The IMPACT Solar Wind Electron Analyzer (SWEA), *The STEREO Mission*, edited by C. T. Russell, pp. 227–239, Springer, New York, doi:10.1007/978-0-387-09649-0_9.

Sheeley, N. R., Jr., et al. (1997), Measurements of flow speeds in the corona between 2 and 30 R$_\odot$, *Astrophys. J.*, *484*, 472, doi:10.1086/304338.

Simunac, K. D. C., et al. (2009), In situ observations of solar wind stream interface evolution, *Sol. Phys.*, *259*(1–2), 323–344, doi:10.1007/s11207-009-9393-y.

Smith, C. W., J. L'Heureux, N. F. Ness, M. H. Acuña, L. F. Burlaga, and J. Scheifele (1998), The ACE magnetic fields experiment, *Space Sci. Rev.*, *86*, 613–632, doi:10.1023/A:1005092216668.

Song, H. Q., Y. Chen, K. Liu, S. W. Feng, and L. D. Xia (2009), Quasi-periodic releases of streamer blobs and velocity variability of the slow solar wind near the Sun, *Sol. Phys.*, *258*, 129–140.

Song, H. Q., Z. Zhong, Y. Chen, J. Zhang, X. Cheng, L. Zhao, Q. Hu, and G. Li (2016), A statistical study of the average iron charge state distributions inside magnetic clouds for solar cycle 23, *Astrophys. J. Suppl. Ser.*, *224*(2), 27.

Suess, S. T., Y.-K. Ko, R. von Steiger, and R. L. Moore (2009), Quiescent current sheets in the solar wind and origins of slow wind, *J. Geophys. Res.*, *114*, A04103, doi:10.1029/2008JA013704.

Tian, H., S. Yao, Q. Zong, J. He, and Y. Qi (2010), Signatures of magnetic reconnection at boundaries of interplanetary small-scale magnetic flux ropes, *Astrophys. J.*, *720*(1), 454.

von Steiger, R., N. A. Schwadron, L. A. Fisk, J. Geiss, G. Gloeckler, S. Hefti, B. Wilken, R. R. Wimmer-Schweingruber, and T. H. Zurbuchen (2000), Composition of quasi-stationary solar wind flows from Ulysses/solar wind ion composition spectrometer, *J. Geophys. Res.*, *105*(A12), 27,217–27,238, doi:10.1029/1999JA000358.

Wang, C., J. D. Richardson, L. F. Burlaga, and N. F. Ness (2003), On radial heliospheric magnetic fields: Voyager 2 observation and model, *J. Geophys. Res.*, *108*(A5), 1205, doi:10.1029/2002JA009809.

Wang, Y., B. Zhuang, Q. Hu, R. Liu, C. Shen, and Y. Chi (2016), On the twists of interplanetary magnetic flux ropes observed at 1 AU, *J. Geophys. Res. Space Physics*, *121*, 9316–9339, doi:10.1002/2016JA023075.

Wang, Y. M., N. R. Sheeley Jr., J. H. Walters, G. E. Brueckner, R. A. Howard, D. J. Michels, P. L. Lamy, R. Schwenn, and G. M. Simnett (1998), Origin of streamer material in the outer corona, *Astrophys. J.*, *498*, L165.

Wang, Y. M., N. R. Sheeley Jr., D. G. Socker, R. A. Howard, and N. B. Rich (2000), The dynamical nature of coronal streamers, *J. Geophys. Res.*, *105*(A11), 25,133–25,142, doi:10.1029/2000JA000149.

Wimmer-schweingruber, R. F., and D. M. Hassler (2016), Tracing heliospheric structures to their solar origin, in *Solar Wind Fourteen*, *AIP Conf. Proc.*, vol. 1720, 100002-1–100002-4, doi:10.1063/1.4943857.

Winterhalter, D., E. J. Smith, M. E. Burton, N. Murphy, and D. J. McComas (1994), The heliospheric plasma sheet, *J. Geophys. Res.*, *99*(A4), 6667–6680, doi:10.1029/93JA03481.

Yu, W., et al. (2014), A statistical analysis of properties of small transients in the solar wind 2007-2009: STEREO and Wind observations, *J. Geophys. Res. Space Physics*, *119*, 689–708, doi:10.1002/2013JA019115.

Yu, W., C. J. Farrugia, A. B. Galvin, N. Lugaz, J. G. Luhmann, K. D. C. Simunac, and E. Kilpua (2016), Small solar wind transients at 1 AU: STEREO observations (2007–2014) and comparison with near-Earth wind results (1995–2014), *J. Geophys. Res. Space Physics*, *121*, doi:10.1002/2016JA022642.

Zhao, L., T. H. Zurbuchen, and L. A. Fisk (2009), Global distribution of the solar wind during solar cycle 23: ACE observations, *Geophys. Res. Lett.*, *36*, L14104, doi:10.1029/2009GL039181.

Zhao, L., E. Landi, T. H. Zurbuchen, L. A. Fisk, and S. T. Lepri (2014), The evolution of 1 AU equatorial solar wind and its association with the morphology of the heliospheric current sheet from solar cycle 23 to 24, *Astrophys. J.*, doi:10.1088/0004-637X/793/1/44.